Journal of Materials Processing Tech. 252 (2018) 604–611

High performance gravity cast Al9Si0.45Mg0.4Cu alloy inoculated with AlB2 and TiB2

Xixi Dong, Yijie Zhang, Sajjad Amirkhanlou, Shouxun Ji*
Brunel Centre for Advanced Solidification Technology (BAST), Brunel University London, Uxbridge, Middlesex, UB8 3PH, United Kingdom
* Corresponding author.
E-mail address: shouxun.ji@brunel.ac.uk (S. Ji).

Keywords:
Aluminium alloys; Casting; Inoculation process; Mechanical properties; Precipitation strengthening; Defect control

ABSTRACT
The primary α–Al grain size was 540 ± 110 μm in the Al9Si0.45Mg0.4Cu alloy refined by conventional Al5Ti1B master alloy, and that was 340 ± 80 μm in the Al3Ti3B refined alloy. The yield strength, tensile strength and elongation of the T6 heat–treated alloy refined by Al3Ti3B were 320 ± 2 MPa, 375 ± 10 MPa and 6.0 ± 1.0% respectively, which were increased by 3%, 4% and 50% in comparison with the alloy refined by Al5Ti1B. β”, Q' and θ' precipitates were verified for peak strengthening of the heat–treated alloys. The majority of precipitates were β” and Q’, while the minority was θ'. The volume of porosity was decreased by 50% in the Al3Ti3B refined alloy comparing with the Al5Ti1B refined alloy. The inoculation of AlB2 along with TiB2 results in the better grain refinement under Al3Ti3B, which contributes to the enhancement of yield strength and reduction of porosity. The improvement of tensile strength and ductility in Al3Ti3B refined alloy is attributed to the decrease of the size and area fraction of porosity on the fracture surface.

1. Introduction

Li et al. (2013) and Dong et al. (2015a,b) reported that the mechanical properties of AlSi7Mg alloy could be improved by effective grain refinement. The similar results were reported by Samuel et al. (2014) for Al–Si–Mg cast alloys. Dong et al. (2014) reported the enhancement of strength in AlSi9Cu alloy with fine grain size. Zhang et al. (2017) reported the enhancement of mechanical properties in Al–Si alloys under effective grain refinement. As an effective grain refiner, Al5Ti1B master alloy has been widely used in industry over the past several decades. It can offer remarkable refinements in wrought alloys, but it is still difficult to meet the expectations in cast Al–Si alloys with a Si content higher than 3.5 wt.%, as reported by Birol (2012a,b).

Dong et al. (2017) reported a high strength and ductility Al9SiMg cast aluminium alloy with increased Si content. Li et al. (2006) reported that the addition of Cu to Al–Si–Mg alloys was capable of forming new precipitates to increase the strength. Shabestari and Moemeni (2004) studied the effects of Cu on the microstructure and mechanical properties of AlSi7Mg alloys. Paray et al. (2000) reported that high Cu contents could significantly increase the hot tearing susceptibility, and Zor et al. (2010) reported that high Cu contents could also increase the intergranular corrosion, in Al–Si–Mg alloys. The Cu contents below 0.5 wt.% is necessary to prevent hot tearing and intergranular corrosion. There are two major concerns for the cast Al–Si–Mg alloys with increased Si and Cu. One concern is

the decrease of efficiency of grain refinement using Al5Ti1B in high Si aluminium alloys. The reason is that the Si in the melt reacts with Ti to form Ti–Si phases, which poison the TiB2 nucleation sites, as reported by Qiu et al. (2007). One possible solution is to increase the B content in the grain refiners, as given by Birol (2009, 2012a,b). The other concern is the decrease of ductility due to the increase of porosity after the addition of Cu, as reported by Zheng et al. (2015). Zuo et al. (2011) and Dong et al. (2015a,b) reported that efficient grain refinement could decrease the porosity in cast aluminium alloys, which is beneficial to ductility. Efficient grain refinement could be considered as a solution to overcome the grain refining and porosity problems accompanied with the high silicon and low copper Al–-Si–Mg–Cu cast alloys.

The present paper aims to study the cast Al9Si0.45Mg0.4Cu alloy for providing high strength and ductility. Al3Ti3B master alloy containing AlB2 and TiB2 was used for effective grain refinement in the high Si alloys. The microstructure and tensile properties of the Al9Si0.45Mg0.4Cu alloy under inoculation of AlB2 and TiB2 were investigated and compared with the non–refined and conventional Al5Ti1B refined condition, and the enhancement mechanisms of grain refinement and mechanical properties were studied and discussed.

2. Experimental

2.1. Grain refiner preparation

The grain refiner of AlB2 and TiB2 was made in Al3Ti3B master alloy, which was synthesised in the lab using halide salt process, as reported by Birol (2011). The Al3Ti3B master alloys were made by adding K2TiF6 and KBF4 into molten aluminium with predefined ratio at 800 °C for 20 min. The master alloy was examined by the D8 X-ray diffraction (XRD) diffractometer equipped with Cu Kα radiation. The XRD analysis was conducted for the 2θ degrees from 25° to 90° at a scanning speed of 1°/min. As shown in Fig. 1, TiB2 and AlB2 were found, and no TiAl3 were found, in the Al3Ti3B master alloy. AlB2 and TiB2 are insoluble in aluminium melt, and Birol (2012a,b) reported that both of them could act as heterogeneous nucleation sites for α–Al. For comparison, commercial Al5Ti1B master alloy was used as grain refiner to make samples for the same alloy.

2.2. Melt preparation

The baseline alloy A0, with the composition listed in Table 1, was melted in a 12–kg capacity clay–graphite crucible using an electric resistance furnace. The alloying elements were added to the A0 melt to get the desired compositions of A1, A2 and A3, where magnesium was added in the pure ingot, silicon and copper were added in the form of Al–50 wt.% Si and Al–50 wt.% Cu master alloys, respectively. During melting, the temperature of the furnace was controlled at 750 °C. After one hour of homogenisation, Al–10 wt.% Sr master alloy was added into the melt for modification. The melt was subsequently degassed through injecting pure argon into the melt by using a rotary degassing impeller at a speed of 350 rpm for 4 min. After degassing, the top surface of the melt was covered by commercial granular flux, and the melt was hold for 10 min for temperature recovery, followed by casting without grain refinement (GR), or adding 0.2 wt.% Al5Ti1B or 0.2 wt.% Al3Ti3B master alloys into the melt for grain refinement before casting. Mushroom samples were made for composition analysis. The chemical compositions of the alloys were measured by inductively coupled plasma atomic emission spectroscopy (ICP–AES) and listed in Table 1.

2.3. Casting process and heat treatment

With the intention of casting tensile test bars, the prepared melt was poured at 720 °C into a permanent mould, which was made according to ASTM B–108, and two tensile test bars were made from each casting, as shown in Fig. 2(a). Fig. 2(b) shows the key dimensions of the gravity casting tensile test bar made by the permanent mould. The mould was preheated to 460 °C before casting. Eight castings were made one after one in 20 min for each of the non–refined, Al5Ti1B refined and Al3Ti3B refined condition. After kept at ambient condition for at least 24 h, the cast tensile test bars were subjected to T6 heat treatment, including solution treatment and artificial aging. Solution treatment was carried out at 504 °C for 2 h in the first stage for the solution of the θ–Al2Cu phase and 535 °C for 6 h in the second stage for the solution of the Q–Al5Cu2Mg8Si6 phase, followed by immediate water quenching to room temperature. Four hours after quenching, aging treatment was performed at 170 °C for 12 h, followed by air cooling to room temperature.

2.4. Characterization

The specimens for microstructure examination were cut from the middle of φ10 mm round tensile test bars. The microstructure was examined using the Zeiss optical microscopy (OM), the Zeiss SUPRA 35VP scanning electron microscope (SEM) equipped with energy dispersive X-ray spectroscopy (EDS), the JEOL–2100 transmission electron microscopy (TEM). The specimens for OM, SEM and XRD analysis were prepared by the standard technique of grinding. OM observation was conducted after polishing without any etching. Polarized OM observation of grain size was performed after anodised with Barker solution (97vol.% H2O and 3 vol.% HBF4). SEM analysis was conducted after etching with 15 vol.% HCl. Thin specimens for TEM observation were prepared by standard electropolishing. The electrolytic solution was a mixture of nitric acid and methyl alcohol (1:3), used at −20 to −30 °C and 20 V. TEM operating at 200 kV was used for bright field imaging, select area diffraction pattern (SADP) analysis, and high–resolution transmission electron microscopy (HRTEM) imaging. Tensile tests were conducted following the ASTM B557 standard using an Instron 5500 Universal Electromechanical Testing Systems. All the tensile tests were performed at room temperature. The gauge length of the extensometer was 50 mm and the ramp rate for extension was 1 mm/min. Each data reported with standard deviation was based on the properties obtained from 6 to 8 samples.

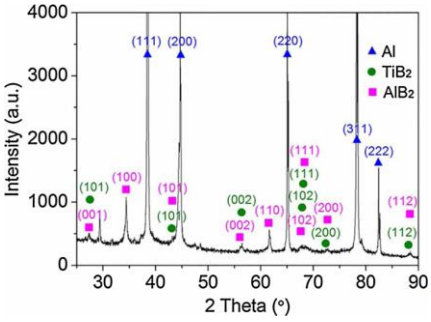

Fig. 1. X-ray diffraction pattern of the Al3Ti3B master alloy made for grain refinement.

Table 1 Chemical compositions of experimental alloys analyzed by ICP–AES (wt.%).

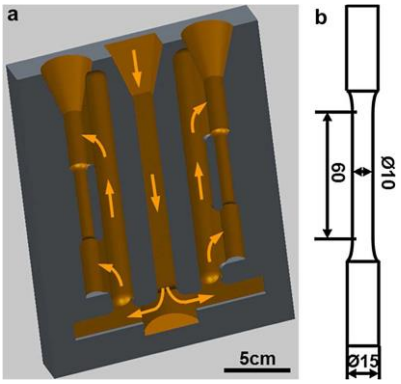

Fig. 2. (a) Permanent mould made according to ASTM B–108, and (b) key dimensions of the gravity casting tensile test bar made by the mould.

3. Results

3.1. As–cast microstructure

Fig. 3(a)–(c) present the SEM morphology of the as–cast Al9-Si0.45Mg0.4Cu alloys without grain refinement and refined by Al5Ti1B and Al3Ti3B master alloys, separately. The main phases are the primary α – Al phase and the Al–Si eutectic phase. The primary α–Al phase in the Al3Ti3B refined alloy is much finer than that in the non–refined and Al5Ti1B refined alloys. No coarse plate–like eutectic Si phase was observed in the alloys, which indicated that the eutectic Si phase was well modified. Three intermetallic phases were identified in the as–cast Al9Si0.45Mg0.4Cu alloys, i.e., β–Mg2Si phase, Q–Al5Cu2Mg8Si6 phase and θ–Al2Cu phase, as indicated by the arrows in Fig. 3. β–Mg2Si phase is located in the eutectic Si region, and the grey phase was identified as the Q–Al5Cu2Mg8Si6 phase with block shapes, while the light phase was identified as the θ–Al2Cu phase, which were consistent with that reported by Zheng et al. (2015).

Fig. 4(a)–(c) show the SEM micrographs of the eutectic Si phase in the as–cast Al9Si0.45Mg0.4Cu alloys without grain refinement and refined by Al5Ti1B and Al3Ti3B master alloys, respectively. The eutectic Si phase was well modified to fine fibrous structure with small aspect ratios, and the eutectic Si phases in the as–cast alloys under the three grain refinement condition are much similar to each other. Xu et al. (2015a,b) reported that the eutectic Si phase in unmodified Al–Si alloys was coarse plate–like structure with high aspect ratio that could be over 27, which is prone to induce crack under loading. The refined eutectic Si fibres are desirable to obtain a fine microstructure after solution treatment, and it is beneficial to the mechanical properties especially ductility after heat treatment.

3.2. Microstructure after heat treatment

Fig. 5(a)–(c) show the SEM morphology of the Al9Si0.45Mg0.4Cu alloys without grain refinement and refined by Al5Ti1B and Al3Ti3B master alloys, separately, after T6 heat treatment. The primary α–Al phase and the spheroidised Si particles were clearly visible, but the intermetallic phases were hardly observed in the microstructure under the three grain refinement condition, indicating that the β–Mg2Si, Q–Al5Cu2Mg8Si6 and θ–Al2Cu intermetallic phases were well dissolved into the α–Al matrix after solution treatment. Similar to the as–cast condition, the primary α–Al phase in the T6 heat–treated alloy refined by Al3Ti3B is much finer than that in the non–refined and Al5Ti1B refined

alloys, since T6 heat treatment hardly has any effect on the size and morphology of the primary α–Al phase. The saturated solid solution could ensure the precipitation of nanoscale strengthening precipitates in the α–Al matrix during the aging treatment, which strengthens the alloys.
Fig. 6(a)–(c) show the SEM morphology of the eutectic Si phase in the Al9Si0.45Mg0.4Cu alloys without grain refinement and refined by Al5Ti1B and Al3Ti3B master alloys, respectively, after solution and aging treatment. The eutectic Si phase shows spheroidal morphology, and it is different to the fibrous morphology observed in Fig. 4 under the as–cast condition. The spheroidised Si particles in the heat–treated alloys under the three grain refinement condition are much similar to each other, with the size smaller than 8 μm and the aspect ratio smaller than 2.5. The spheroidised fine Si particles are resulted from the fusing of fibrous Si during solution treatment, which are reported by Xu et al. (2015a,b) beneficial to the mechanical properties especially ductility.

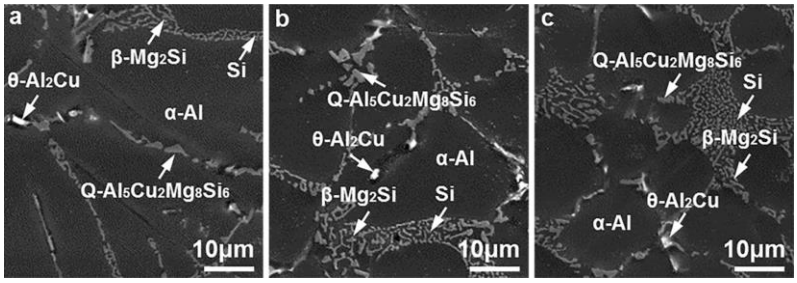

Fig. 3. SEM micrographs showing the morphology of the as–cast Al9Si0.45Mg0.4Cu alloys refined by (a) No refinement, (b) Al5Ti1B and (c) Al3Ti3B.

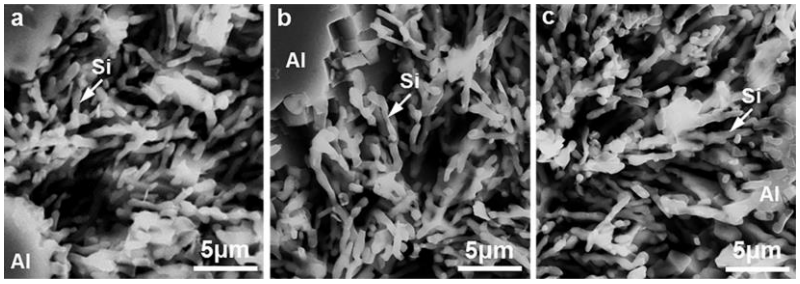

Fig. 4. SEM micrographs showing the morphology of eutectic Si phase in the as–cast A9Si0.45Mg0.4Cu alloys refined by (a) No refinement, (b) Al5Ti1B and (c) Al3Ti3B.

3.3. Enhancement of grain refinement

Fig. 7(a)–(c) present the polarized optical micrographs showing the grain size of primary α–Al phase in the as–cast Al9Si0.45Mg0.4Cu alloys without grain refinement and refined by Al5Ti1B and Al3Ti3B master alloys, respectively. The primary α–Al phase shows coarse dendritic morphology in the as–cast Al9Si0.45Mg0.4Cu alloy without grain refinement and refined by Al5Ti1B. The primary α–Al phase in the as–cast Al9Si0.45Mg0.4Cu alloy refined by Al3Ti3B is finer than the non–refined and Al5Ti1B refined condition. Fig. 7(d) and (e) show the statistical distribution of grain size and statistical average grain size of primary α–Al phase in the as–cast Al9Si0.45Mg0.4Cu alloys under the three grain refinement condition, separately. More than 300 grains were counted to give the statistical results under each grain refinement condition. From Fig. 7(d), the grain size shows lognormal distribution, and the majority of the primary α–Al phase in the Al3Ti3B refined alloy is much finer than that in the non–refined and Al5Ti1B refined alloys.

From Fig. 7(e), the grain size of the primary α–Al phase is 800 ± 200 μm without grain refinement, and that is 540 ± 110 μm when refined by Al5Ti1B, while that is 340 ± 80 μm when refined by Al3Ti3B. The grain size of primary α–Al phase in the Al3Ti3B refined alloy is reduced by 40%, when compared with the Al5Ti1B refined alloy. Al3Ti3B is more effective grain refiner for the Al9Si0.45Mg0.4Cu cast alloy than Al5Ti1B.

3.4. Enhancement of mechanical properties

The Al9Si0.45Mg0.4Cu alloy is heat treatment strengthening alloy, so its mechanical properties after heat treatment were focused rather than the as–cast mechanical properties. Fig. 8 shows the typical tensile stress–strain curves and tensile properties of the Al9Si0.45Mg0.4Cu alloys under different grain refinements, after T6 heat treatment. The alloys with grain refinement showed higher strength and ductility than the non–refined alloy, in which the alloy refined by Al3Ti3B offered the best strength and ductility. The yield strength (YS), tensile strength (TS) and elongation (El) of the non–refined alloy were 305 ± 2 MPa, 350 ± 3 MPa and 3.0 ± 0.5%, respectively. The Al5Ti1B refined alloy provided the YS of 310 ± 2 MPa and the UTS of 360 ± 5 MPa, and the El of 4.0 ± 1.0%. When the alloy was refined by Al3Ti3B, the YS was 320 ± 2 MPa, the UTS was 375 ± 10 MPa and the El was 6.0 ± 1.0%. The strength could be increased, and the elongation could be increased by 50% in the Al3Ti3B refined alloy, when compared with the Al5Ti1B refined alloy.

4. Discussion

4.1. Enhancement mechanism of grain refinement

Fig. 9 shows the XRD patterns of the Al5Ti1B master alloy used for refinement, TiAl3 and TiB2 were found coexisting in the Al5Ti1B master alloy. The soluble TiAl3 and the insoluble TiB2 were well documented introducing into the melt under the addition of the Al5Ti1B grain refiner, which is consistent with the XRD results shown in Fig. 9. Fan et al. (2015) reported that (0001) planes of TiB2 could act as heterogeneous nucleation sites for (111) planes of α–Al crystals. Mohanty and Gruzleski (1996) reported that these basal planes of TiB2 could be poisoned by Si by coating the surfaces with Ti–Si compounds. The dissolved Ti from TiAl3, which also contributes to grain refinement under Al5Ti1B by slowing down the growth of the freshly formed α–Al crystals while partitioning between the solid and liquid phases, is also rendered ineffective as it also forms Ti–Si compounds and precipitates out of the melt. Birol (2012a,b) reported that solute Ti hardly offered any grain refinement effect in Al–Si alloys with 7 wt.% Si. The Al9- Si0.45Mg0.4Cu cast alloy contains a high level of Si at 9 wt.%, so the poisoning effect of TiB2 is significant, and the solute Ti might hardly provide growth restriction for the primary α–Al phase, due to the formation of Ti–Si compounds, which result in the coarse primary α–Al grains of 540 ± 110 μm in the alloy refined by Al5Ti1B. Chen et al. (2016) reported that AlB2 could also act as heterogeneous nucleation sites for α–Al, so the XRD results shown in Fig. 1 indicate that the Al3Ti3B master alloy relies on the insoluble AlB2 and TiB2 borides to promote heterogeneous nucleation of the primary α–Al phase. Borides in the Al3Ti3B grain refiner are nearly three times as many as that in Al5Ti1B, since the B content dictates the population of borides. This was also evidenced by the B content listed in Table 1. Thus the performance of the Al3Ti3B for the refinement of the high silicon and low copper Al9Si0.45Mg0.4Cu cast alloy is clearly superior with respect to that of Al5Ti1B, as shown in Fig. 7. The inoculation of AlB2 is mainly credited for this improvement since the TiB2 suffer from Si poisoning. TiB2 still

contribute to the heterogeneous nucleation of the primary α－Al phase though suffering from Si poisoning, since the grain size of the Al5Ti1B refined alloy is lower than that of the non–refined alloy, as shown in Fig. 7. The inoculation of AlB2 along with TiB2 results in the effective grain refinement under Al3Ti3B.

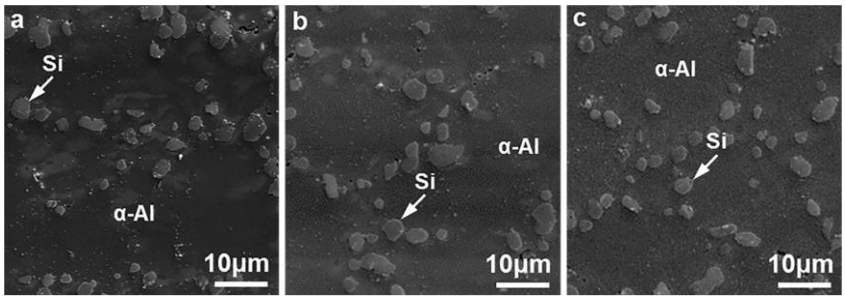

Fig. 5. SEM micrographs showing the morphology of the T6 heat–treated Al9Si0.45Mg0.4Cu alloys refined by (a) No refinement, (b) Al5Ti1B and (c) Al3Ti3B.

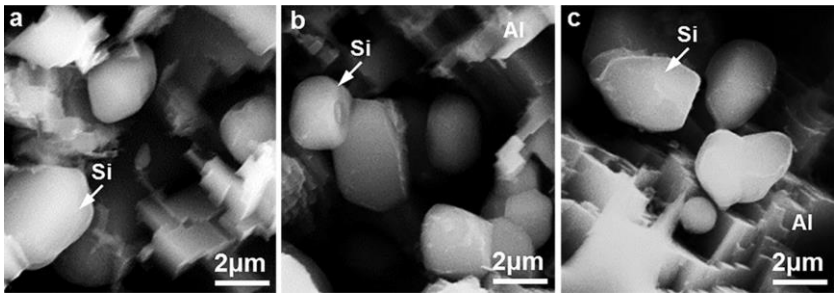

Fig. 6. SEM micrographs showing the morphology of eutectic Si phase in the T6 heat–treated Al9Si0.45Mg0.4Cu alloys refined by (a) No refinement, (b) Al5Ti1 and (c) Al3Ti3B.

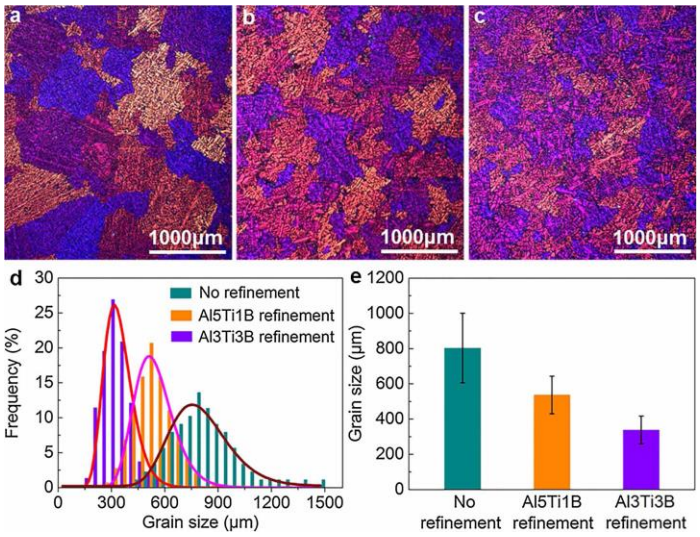

Fig. 7. Polarized optical micrographs showing the grain size of primary α–Al phase in the as–cast Al9Si0.45Mg0.4Cu alloys refined by (a) No refinement, (b) Al5Ti1B, (c) Al3Ti3B, and (d) statistical distribution of grain size and (e) statistical average grain size.

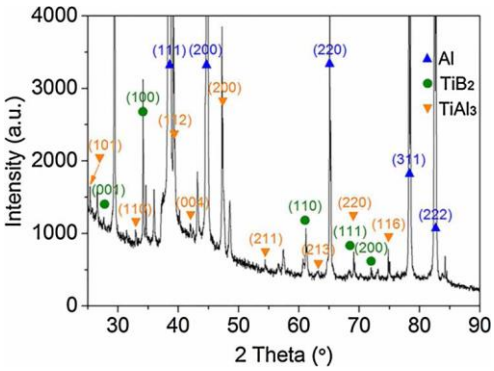

Fig. 8. (a) Typical tensile stress–strain curves and (b) tensile properties of the Al9Si0.45Mg0.4Cu alloys after T6 heat treatment.

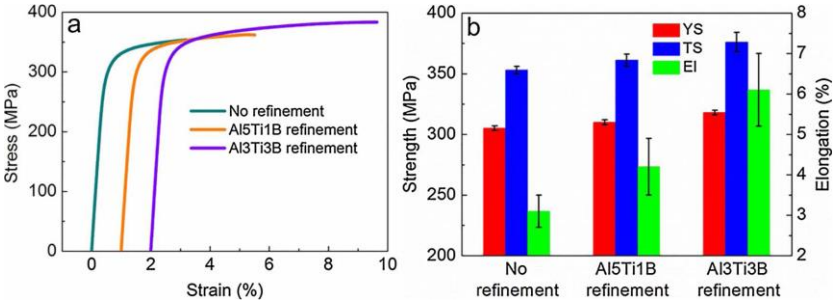

Fig. 9. X-ray diffraction pattern of the Al5Ti1B master alloy used for grain refinement.

4.2. Enhancement mechanism of yield strength

Fig. 10 presents the TEM micrographs taken along the ⟨001⟩Al axis showing precipitates in the Al9Si0.45Mg0.4Cu alloy after T6 heat treatment. Fig. 9(a) shows the bright field image of precipitates in the α－Al matrix, β”, Q' and θ' precipitates were found coexisting, as indicated by the arrows. By multiple fields observation, the majority of precipitates are β” and Q', while the θ' precipitate is in the minority. The up–right corner insert in Fig. 10(a) shows the SADP of α–Al matrix and precipitates, the bright points are diffraction points of the α–Al matrix, while the grey cross lines between the bright points are diffraction patterns of precipitates, which indicate that the precipitates are in the metastable state and the heat–treated alloy is in the peak strength state. Fig. 10(b) and (c) show the HRTEM images of the β” and Q' precipitates lying on the (001)Al plane, and the up–right corner fast Fourier transform (FFT) patterns in Fig. 10(b) and (c) verify that the lying precipitates are β” and Q', respectively. Fig. 10(d) presents the HRTEM image of the θ' precipitate on the (001)Al plane, and the up–right corner FFT pattern proves that the precipitate is θ'. The needle–like β” precipitate is coherent with α–Al matrix, as reported by Yang et al. (2012, 2014). The lath shaped Q' and plate shaped θ' precipitates are semi–-coherent with the α–Al matrix, as reported by Xiao et al. (2017). These precipitates could provide excellent precipitation strengthening effect, which ensures the peak strengthening of the alloy, and contributes to the high yield strength of above 305 MPa for the alloy after heattreatment.

The yield strength of the T6 heat–treated Al9Si0.45Mg0.4Cu cast alloys is dependent on the grain size of the primary α–Al phase, the spheroidised secondary Si phase and the precipitation phases. From Figs. 5 and 6, the spheroidised Si particles in the alloys under the three grain refinement condition are much similar. There was nearly no difference for the β”, Q' and θ' precipitation phases

in the α–Al matrix of the alloys under the three grain refinement condition by TEM observation. Thus the increase of yield strength in the Al3Ti3B refined alloy can be attributed to better grain refinement of the primary α–Al phase.

4.3. Enhancement mechanism of tensile strength and ductility

The tensile strength and ductility of the T6 heat treated cast Al–Si–Mg alloys free from porosity or other casting defects depend on the scale of the dendritic structure and the size and shape of the Si particles, as reported by Cáceres et al. (1995), Cáceres and Griffiths (1996) . The tensile strength and ductility of the T6 heat treated cast Al–Si–Mg alloys with defects present is determined by the size and area fraction of defects on the fracture surface, rather than the bulk volume percentage of defects. Surappa et al. (1986) pointed out that the tensile strength and ductility of the T6 heat treated Al–7Si–0.3Mg cast alloy depend mainly on the size of the macropores on the fracture surface, rather than on the volume percentage of porosity obtained by density measurement. Cáceres and Selling (1996) reported that the tensile strength and ductility of the T6 heat treated Al–7Si–0.4Mg cast alloy showed correlation with the area fraction of defects on the fracture surface rather than the bulk porosity content, and the tensile strength and ductility decreases monotonically with an increase in the area fraction of defects on the fracture surface.

Fig. 11(a–(c) show the SEM images of porosity defect on the fracture surface of the T6 heat–treated Al9Si0.45Mg0.4Cu alloys without grain refinement and refined by Al5Ti1B and Al3Ti3B master alloys, respectively. Porosity defect presents in the T6 heat–treated Al9-Si0.45Mg0.4Cu alloys, so the tensile strength and ductility of the alloys depend on the size and area fraction of porosity on the fracture surface. The size and area fraction of porosity on the fracture surface of the Al3Ti3B refined alloy is smaller than that of the non–refined and Al5Ti1B refined alloys, which results in the improvement of the tensile strength and ductility in the Al3Ti3B refined alloy. Fig. 11(d) presents the volume percentage of porosity in the Al9Si0.45Mg0.4Cu alloys under the three grain refinement condition. The volume percentage of porosity in the non–refined and Al5Ti1B refined alloys is 0.4% and 0.2%, and that is decreased to 0.1% in the Al3Ti3B refined alloy. The trend of the volume percentage of porosity in the alloys is consistent with the size and area fraction of porosity on the fracture surface, but the decrease of the size and area fraction of porosity on the fracture surface determines the enhancement of tensile strength and ductility in the Al3Ti3B refined alloy, rather than the decrease of the bulk volume percentage of porosity.

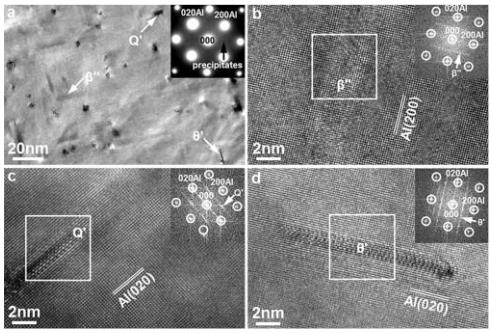

Fig. 10. TEM micrographs showing precipitates in the T6 heat–treated Al9Si0.45Mg0.4Cu alloy, (a) bright field image, and high resolution TEM images of (b) β”, (c) Q', and (d) θ' precipitates observed along the ⟨001⟩Al axis.

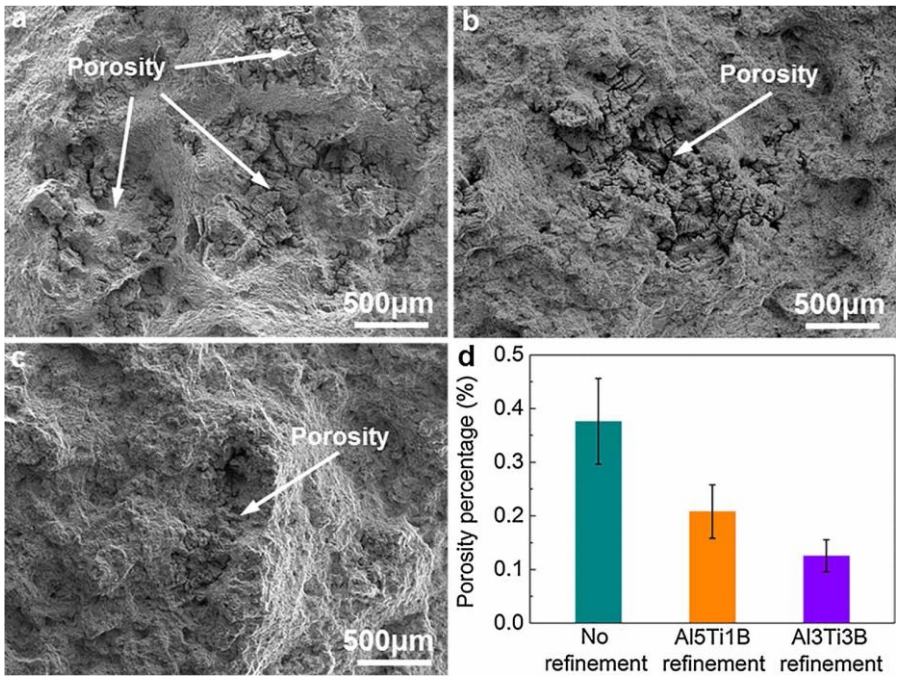

Fig. 11. SEM micrographs showing the porosity on the fracture surface of the T6 heat–treated Al9Si0.45Mg0.4Cu alloys refined by (a) No refinement, (b) Al5Ti1B and (c) Al3Ti3B, and (d) volume percentage of porosity.

The primary α–Al phase is dendrite morphology with several dendrite arms in hypoeutectic cast Al–Si alloys, and the dendrite arms will impede the entry of the remaining liquid into the intervals between dendrite arms during solidification. Porosity forms when the remaining liquid can't compensate the interval wrapped by well-developed primary α－Al dendrite arms. Grain refinement of the primary α–Al phase is well understood beneficial in reducing porosity in cast Al alloys, as reported by Zuo et al. (2011). The reason is that the remaining liquid is easier to compensate the intervals between fine primary α–Al dendrites, while it is difficult to compensate the intervals between coarse primary α－Al dendrites. As shown in Fig. 7, the primary α–Al dendrite in the Al3Ti3B refined alloy is finer than that in the non–refined and Al5Ti1B refined alloys, which results in the decrease of the porosity in the Al3Ti3B refined alloy comparing with the non–refined and Al5Ti1B refined alloys. The improvement of tensile strength and ductility in Al3Ti3B refined alloy is attributed to the decrease of the size and area fraction of porosity on the fracture surface under efficient grain refinement.

5. Conclusions

(1) TiB2 and AlB2 are inoculated for grain refinement under Al3Ti3B. Al3Ti3B is more effective than Al5Ti1B for the grain refinement of the Al9Si0.45Mg0.4Cu alloy. The grain size of primary α–Al phase is 800 ± 200 μm, 540 ± 110 μm and 340 ± 80 μm in the non–refined, Al5Ti1B refined and Al3Ti3B refined alloys, respectively.

(2) The yield strength, tensile strength and elongation of the T6 heat–treated Al9Si0.45Mg0.4Cu alloy refined by Al3Ti3B were 320 ± 2 MPa, 375 ± 10 MPa and 6.0 ± 1.0% respectively, which were increased by 3%, 4% and 50% in comparison with the alloy refined by Al5Ti1B.

(3) β”, Q' and θ' phases are precipitated from the α–Al matrix for the peak strengthening of the T6 heat–treated Al9Si0.45Mg0.4Cu alloy, β ” and Q' precipitates exist as the majority, and the θ' precipitate exists as the minority.

(4) The increase of yield strength in the Al3Ti3B refined Al9Si0.45Mg0.4Cu alloy results from the efficient refinement. The improvement of tensile strength and ductility in Al3Ti3B refined alloy is attributed to the reduction of the size and area fraction of porosity on the fracture surface under efficient grain refinement.

Acknowledgements
Financial support from Innovate UK under project 131817 is gratefully acknowledged. Instruction for the discussion of the improvement of tensile strength and ductility from the subject editor Dr C.H. Cáceres is gratefully acknowledged. Professor S.S. Wu is gratefully acknowledged for the critical reading of the paper. The National Natural Science Foundation of China (51501152) and Natural Science Basic Research Plan in Shaanxi Province of China (2016JQ5093) are also gratefully acknowledged.

References
Birol, Y., 2009. A novel Al–Ti–B alloy for grain refining Al–Si foundry alloys. J. Alloy Compd. 486, 219–222.
Birol, Y., 2011. Improved halide salt process to produce Al-B master alloys. Mater. Sci. Technol. 27, 1846–1850.
Birol, Y., 2012a. Effect of silicon content in grain refining hypoeutectic Al–Si foundry alloys with boron and titanium additions. Mater. Sci. Technol. 28, 385–389.
Birol, Y., 2012b. Performance of AlTi5B1, AlTi3B3 and AlB3 master alloys in refining grain structure of aluminium foundry alloys. Mater. Sci. Technol. 28, 481–486.
Cáceres, C.H., Griffiths, J.R., 1996. Damage by the cracking of silicon particles in an Al–7Si–0. 4Mg casting alloy. Acta Mater. 44, 25–33.
Cáceres, C.H., Selling, B.I., 1996. Casting defects and the tensile properties of an Al–Si–Mg alloy. Mater. Sci. Eng. A 220, 109–116.
Cáceres, C.H., Davidson, C.J., Griffiths, J.R., 1995. The deformation and fracture behaviour of an Al–Si–Mg casting alloy. Mater. Sci. Eng. A 197, 171–179.
Chen, Z.N., Kang, H.J., Fan, G.H., Li, J.H., Lu, Y.P., Jie, J.C., Zhang, Y.B., Li, T.J., Jian, X.G., Wang, T.M., 2016. Grain refinement of hypoeutectic Al-Si alloys with B. Acta Mater. 120, 168–178.
Dong, X.X., He, L.J., Li, P.J., 2014. Gradient microstructure and multiple mechanical properties of AlSi9Cu alloy ribbon produced by melt spinning. J. Alloy Compd. 612, 20–25.
Dong, X.X., He, L.J., Huang, X.S., Li, P.J., 2015a. Effect of electromagnetic transport process on the improvement of hydrogen porosity defect in A380 aluminum alloy. Int. J. Hydrogen Energy 40, 9287–9297.
Dong, X.X., He, L.J., Mi, G.B., Li, P.J., 2015b. Two directional microstructure and effects of nanoscale dispersed Si particles on microhardness and tensile properties of AlSi7Mg melt-spun alloy. J. Alloy Compd. 618, 609–614.

Dong, X.X., Zhang, Y.J., Ji, S.X., 2017. Enhancement of mechanical properties in high silicon gravity cast AlSi9Mg alloy refined by Al3Ti3B master alloy. Mater. Sci. Eng. A 700, 291–300.
Fan, Z., Wang, Y., Zhang, Y., Qin, T., Zhou, X.R., Thompson, G.E., Pennycook, T., Hashimoto, T., 2015. Grain refining mechanism in the Al/Al–Ti–B system. Acta Mater. 84, 292–304.
Li, Y.J., Brusethaug, S., Olsen, A., 2006. Influence of Cu on the mechanical properties and precipitation behavior of AlSi7Mg0.5 alloy during aging treatment. Scr. Mater. 54, 99–103.
Li, P.T., Liu, S.D., Zhang, L.L., Liu, X.F., 2013. Grain refinement of A356 alloy by Al–Ti–B–C master alloy and its effect on mechanical properties. Mater. Des. 47, 522–528.
Mohanty, P.S., Gruzleski, J.E., 1996. Grain refinement mechanisms of hypoeutectic Al-Si alloys. Acta Metall. Mater. 44, 3749–3760.
Paray, F., Kulunk, B., Gruzleski, J.E., 2000. Hot tearing in 319 alloy. Int. J Cast Metal Res. 13, 147–159.
Qiu, D., Taylor, J.A., Zhang, M.X., Kelly, P.M., 2007. A mechanism for the poisoning effect of silicon on the grain refinement of Al–Si alloys. Acta Mater. 55, 1447–1456.
Samuel, E., Golbahar, B., Samuel, A.M., Doty, H.W., Valtierra, S., Samuel, F.H., 2014. Effect of grain refiner on the tensile and impact properties of Al–Si–Mg cast alloys. Mater. Des. 56, 468–479.
Shabestari, S.G., Moemeni, H., 2004. Effect of copper and solidification conditions on the microstructure and mechanical properties of Al-Si-Mg alloys. J. Mater. Process. Technol. 193–198.
Surappa, M.K., Blank, E.W., Jaquet, J.C., 1986. Effect of macro-porosity on the strength and ductility of cast Al-7Si-0.3Mg alloy. Scr. Metall. 20, 1281–1286.
Xiao, Q., Liu, H.Q., Yi, D.Q., Yin, D.Y., Chen, Y.Q., Zhang, Y., Wang, B., 2017. Effect of Cu content on precipitation and age-hardening behavior in Al-Mg-Si-xCu alloys. J. Alloy Compd. 695, 1005–1013.
Xu, C., Xiao, W.L., Hanada, S., Yamagata, H., Ma, C.L., 2015a. The effect of scandium addition on microstructure and mechanical properties of Al-Si-Mg alloy: a multi-refinement modifier. Mater. Charact. 110, 160–169.
Xu, C., Xiao, W.L., Zheng, R.X., Hanada, S., Yamagata, H., Ma, C.L., 2015b. The synergic effects of Sc and Zr on the microstructure and mechanical properties of Al-Si-Mg alloy. Mater. Des. 88, 485–492.
Yang, W.C., Huang, L.P., Zhang, R.R., Wang, M.P., Li, Z., Jia, Y.L., Lei, R.S., Sheng, X.F., 2012. Electron microscopy studies of the age-hardening behaviors in 6005A alloy and microstructural characterizations of precipitates. J. Alloy Compd. 514, 220–233.
Yang, W.C., Ji, S., Huang, L.P., Sheng, X.F., Zhou, L., Wang, M.P., 2014. Initial precipitation and hardening mechanism during non-isothermal aging in an Al-Mg-Si-Cu 6005A alloy. Mater. Charact. 94, 170–177.
Zhang, Y.J., Ji, S., Fan, Z., 2017. Improvement of mechanical properties of Al-Si alloy with effective grain refinement by in-situ integrated Al2.2Ti1B-Mg refiner. J. Alloy Compd. 710, 166–171.
Zheng, Y., Xiao, W.L., Ge, S.J., Zhao, W.T., Hanada, S., Ma, C.L., 2015. Effects of Cu content and Cu/Mg ratio on the microstructure and mechanical properties of Al-Si-Cu-Mg alloys. J. Alloy Compd. 649, 291–296.
Zor, S., Zeren, M., Ozkazanc, H., Karakulak, E., 2010. Effect of Cu content on the corrosion of Al-Si eutectic alloys in acidic solutions. Anticorros Method M 57, 185–191.
Zuo, Y., Li, H., Xia, M., Jiang, B., Scamans, G.M., Fan, Z., 2011. Refining grain structure and porosity of an aluminium alloy with intensive melt shearing. Scr. Mater. 64, 209–212.